Journal of Magnetic Resonance 316 (2020) 106757

Contents lists available at ScienceDirect

Journal of Magnetic Resonance

journal homepage: www.elsevier.com/locate/jmr

Revealing weak histidine ^{15}N homonuclear scalar couplings using Solid-State Magic-Angle-Spinning NMR spectroscopy

Chunhua Tan [a,b], Yuquan Chen [c], Xinhua Peng [c], Zhong Chen [b], Shuhui Cai [b], Timothy A. Cross [a,d], Riqiang Fu [a,*]

[a] National High Magnet Field Lab, 1800 East Paul Dirac Drive, Tallahassee, FL 32310, USA
[b] Department of Electronic Science, Fujian Provincial Key Laboratory of Plasma and Magnetic Resonance, Xiamen University, Xiamen, Fujian 361005, China
[c] CAS Key Laboratory of Microscale Magnetic Resonance and Department of Modern Physics, University of Science and Technology of China, Hefei 230026, China
[d] Department of Chemistry and Biochemistry, Florida State University, Tallahassee, FL 32306, USA

ARTICLE INFO

Article history:
Received 22 February 2020
Revised 12 May 2020
Accepted 27 May 2020
Available online 1 June 2020

Keywords:
Double-spin-echo
J-resolved spectroscopy
Histidine tautomeric states
Hydrogen bonds
Hydrogen-bond mediated *J*-coupling
Solid-state NMR

ABSTRACT

The tautomeric structure and chemistry of the histidine imidazole ring play active roles in many structurally and functionally important proteins and polypeptides. While in NMR spectroscopy histidine chemical shifts (e.g. ^{15}N, ^{13}C, and ^{1}H) have been commonly used to characterize the tautomeric structure, hydrogen bonding, and torsion angles, homonuclear ^{15}N scalar couplings in histidine have rarely been reported. Here, we propose double spin-echo sequences to compare the observed signals with and without a 90° pulse between the two spin-echo periods, such that their signal ratio as a function of the echo time solely depends on homonuclear scalar couplings, allowing for measuring weak homonuclear scalar couplings without influence from transverse dephasing effects, thus capable of revealing hydrogen-bond mediated ^{15}N-^{15}N *J*-couplings that can provide direct and definitive evidence for the formation of N···H···N hydrogen-bonding associated with the imidazole ring. We used two ^{13}C,^{15}N labeled histidine samples recrystallized from solutions at pH 6.3 and pH 11.0 to demonstrate the feasibility of this method and reveal the existence of a weak two-bond scalar coupling between the $N_{\delta1}$ and $N_{\varepsilon2}$ sites in the histidine imidazole ring in three tautomeric states and the presence of a hydrogen-bond mediated scalar coupling between the $N_{\delta1}$ site in the imidazole ring and the backbone N_{α} site in the histidine neutral τ and π states. Our results demonstrate that weak ^{15}N homonuclear scalar couplings can be measured even when their values are less than their corresponding intrinsic natural linewidths, thus providing direct and definitive evidence for the formation of N···H···N hydrogen bonding that is associated with the histidine imidazole ring.

1. Introduction

Histidine is an essential residue in many proteins because of its unique chemistry that it brings to the protein through its structurally flexible imidazole sidechain [1,2]. There are three possible tautomeric states, depending on pH, for histidine imidazole sidechain, as illustrated in Scheme 1. At higher pH values, two neutral tautomers can coexist: the τ tautomer with non-protonated $N_{\delta1}$ and protonated $N_{\varepsilon2}$, and the π tautomer with protonated $N_{\delta1}$ and non-protonated $N_{\varepsilon2}$. While at lower pH values, the imidazole ring becomes charged with both $N_{\delta1}$ and $N_{\varepsilon2}$ protonated. The imidazole side chain has a pKa of approximately 6. At physiological pH different tautomeric states often coexist providing important indications of the biological processes that are taking place in a system. With its imidazole ring serving as a general base and a common coordinating ligand when it is neutral and serving as a general acid and hydrogen-bond donor when in its charged form, histidine plays active roles at physiologically relevant pH values in proteins and peptides [3]. A small shift in physiological pH can influence protonation of the imidazole ring that may be involved in enzyme catalyzed reactions, or assisting in stabilizing protein structure, or mediating proton transfer, and so on. One of the key issues in studying the interactions between the histidine and its surroundings in structurally or functionally active sites is to identify the hydrogen bonding partners for the histidine imidazole rings. For example, the set of four H37 side chains in the pore of the tetrameric M2 protein from *Influenza A* virus is the heart of the H^+ conductance mechanism responsible for H^+ selectivity, pH activation, and interactions with the W41 gate through the protonation and

* Corresponding author.
E-mail address: rfu@magnet.fsu.edu (R. Fu).

https://doi.org/10.1016/j.jmr.2020.106757
1090-7807/

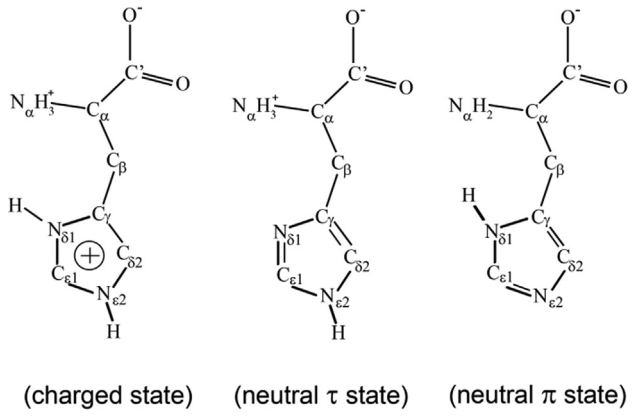

Scheme 1.

deprotonation of the H37 imidazole rings [4,5]. The proton conductance in the M2 channel is facilitated through hydrogen bonds with the His37 residues, in which the basic nitrogen on one imidazole ring can take up a proton to form a charged intermediate and then give up a proton to a solvent molecule before returning to the uncharged state, thus potentially shuttling a proton from one side of a membrane to the other.

It has been known in NMR spectroscopy that both ^{15}N and ^{1}H chemical shifts are very sensitive to hydrogen bonds lengths [6–10] and thus the chemical shifts, including ^{13}C, have been commonly used to characterize the tautomeric structure, hydrogen bonds, and torsion angles of the histidine sidechain. Unfortunately, these chemical shifts are also extremely sensitive to the tautomeric states and the chemical environs of the imidazole rings [8,11,12]. Therefore, the correlation between the ^{15}N and ^{1}H chemical shifts as well as their distance information are required in order to verify the formation of hydrogen bonds [6–11]. It is noteworthy that the measured N···H distance in the hydrogen bond should be shorter than the distance between this nitrogen site and its other nearby protons in the structure due to the dipolar truncation effects. In other words, weak hydrogen bonds that have a longer N···H distance than the shortest distance between this nitrogen site and its nearby protons cannot be verified using the distance measurements. Nevertheless, these approaches are still considered as indirect evidence to affirm the hydrogen bonds.

Scalar couplings (*J*-couplings) arise from an indirect spin-spin interaction between the magnetic dipole moments of the nuclei that are connected through chemical bonds. Thus, *J*-couplings contain a wealth of structural information on the connectivity of chemical bonds and are the basis for many useful methods in solution NMR spectroscopy, such as *i*nsensitive *n*uclei *e*nhanced by *p*olarization *t*ransfer (INEPT) [13] and *i*ncredible *n*atural *a*bundance *d*ouble *qua*ntum *t*ransfer *e*xperiments (INADEQUATE) [14,15]. On the other hand a hydrogen bond is primarily an electrostatic attraction between two polar groups containing highly electronegative atoms such as nitrogen and oxygen that are bridged by a hydrogen atom. Similar to the electron sharing within covalent bonds leading to *J*-couplings [16], the redistribution of electron densities upon hydrogen bond formation acts as electron sharing between the two nuclei involved in the hydrogen bond, although they are not covalently bonded [17], resulting in the so-called hydrogen-bond mediated *J*-couplings [18]. Such *J*-couplings across the hydrogen bonds have been observed in both solution [1,19–22] and solid-state NMR [23–25] spectra and provide direct and definitive evidence for the formation of hydrogen bonds. For the pH-sensitive histidine imidazole ring, the $N_{\delta1}$ nitrogen is always involved in hydrogen bonding. Here, we directly look into the ^{15}N-^{15}N homonuclear *J*-coupling network in the system and use uniformly ^{13}C and ^{15}N labeled histidine samples at pH 6.3 and 11.0 as an example to examine whether or not there exists a two-bond *J*-coupling between $N_{\delta1}$ and $N_{\varepsilon2}$ (i.e. $^{2}J_{N\delta1N\varepsilon2}$) in the imidazole rings and how the backbone nitrogen N_{α} interacts with the $N_{\delta1}$ and $N_{\varepsilon2}$ in the imidazole rings.

Measuring homonuclear *J*-couplings is difficult even in solution NMR, especially when the *J*-couplings are less than the resonance linewidths being observed such that the *J*-splittings are often obscured by signal overlap or buried in the linewidths [26]. While in solid-state NMR, the situation is even worse, since *J*-couplings are much smaller as compared to other spin interactions, such as heteronuclear dipolar interactions. A simple but commonly used method for measuring the *J*-couplings is the so-called *J*-resolved spectra using two-dimensional (2D) spin-echo experiments [23,24,27] that depend on the modulation of *J*-couplings, while refocusing the chemical shifts, thus to generate the *J*-splittings in the spectral indirect dimension. It is generally believed that this method can measure the *J*-coupling constant values that are larger than the natural linewidths (i.e. without other shift contributions such as field inhomogeneity) of the signals being observed. However, in many cases *J*-couplings are quite small, for instance, from those nuclei that are connected through multiple chemical bonds. Particularly in the study of hydrogen bonding, *J*-couplings across hydrogen bonds are typically small but can provide direct evidence about the hydrogen bond formation. In addition, the modulation of the ^{15}N-^{15}N *J*-splittings, if any, can be easily obscured by residual ^{15}N-^{1}H dipolar interactions during the spin-echo period, even under high power ^{1}H decoupling in the 2D spin-echo experiments, thus preventing observation of weak homonuclear ^{15}N-^{15}N *J*-couplings. Selective measurements [28] have been proposed to overcome such spin-spin relaxation effects by using frequency-selective spin-echoes where singly and doubly frequency-selective refocusing pulses are used to generate without and with *J*-modulated spectrum, respectively, such that the ratio of these two spectra depends solely on the *J*-coupling. However, such experiments are highly dependent upon the selectivity of the frequency-selective pulses and may become difficult to perform when the two resonances being investigated are in close proximity.

In this paper, we propose the rotor-synchronized double spin-echo (dubbed as DBSE) sequence [29,30], as shown in Fig. 1, to measure weak *J*-couplings by comparing the signal intensities with and without the 90° pulse sandwiched between the two spin-echo

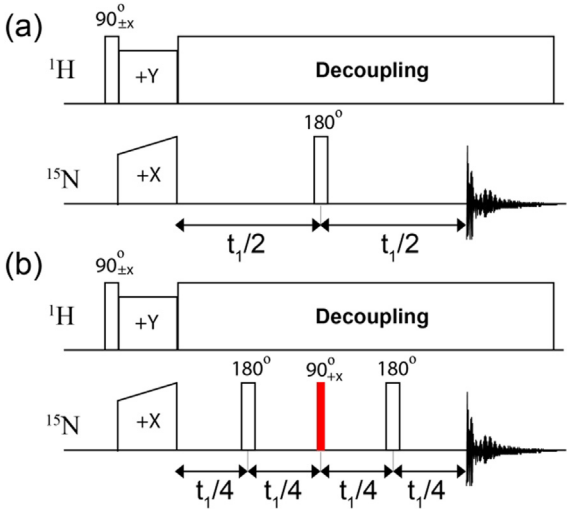

Fig. 1. (a) The standard spin-echo sequence. (b) The double spin-echo pulse sequence. A 90° pulse (in red) is sandwiched by the standard spin-echo sequences.

periods. The double spin-echo sequence was initially proposed in solution NMR [29,30] for simultaneously refocusing both chemical shifts and *J*-couplings (the so-called "perfect echo" for AX systems). Different from the 2D *J*-resolved spectra using the standard spin-echo sequence (c.f. Fig. 1a) where the transverse dephasing (i.e. T_2') also contributes to the line-broadening in the indirect dimension, the ratio of these DBSE signals with and without 90° pulse completely eliminates the transverse dephasing effects, thus allowing us to reveal weak *J*-couplings that cannot be detected by the 2D *J*-resolved spectra. Utilizing such a ratio to remove transverse dephasing effects was not used in the initial double spin-echo experiments in solution [29,30], but has been employed in many MAS NMR experiments [31–34]. We theoretically derived the evolution of *J*-couplings in a three-spin system with and without the 90° pulse in the middle of the two spin echo periods and further use uniformly ^{13}C and ^{15}N labeled histidine samples at pH 6.3 and pH 11.0 to demonstrate the effectiveness of this DBSE sequence. The results reveal the existence of the two-bond $^{2}J_{N\delta1N\varepsilon2}$ value to be as weak as ~1 Hz between $N_{\delta1}$ and $N_{\varepsilon2}$ in the imidazole rings in all three histidine tautomeric states, and the hydrogen-bond mediated $^{2h}J_{N\delta1N\alpha}$ in the neutral states.

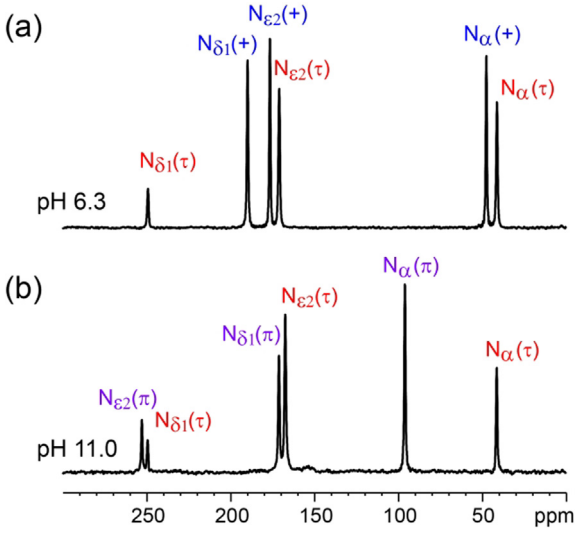

Fig. 2. ^{15}N CPMAS spectra of the His6.3 and His11.0 samples.

2. Material and experimental

Uniformly ^{13}C, ^{15}N-labeled L-Histidine•HCl·H_2O (pH 3.3) was purchased from Cambridge Isotope Laboratories, Inc. and was dissolved in deionized water whose pH was adjusted through adding appropriate volumes of 0.2 M NaOH. Two histidine samples were recrystallized from their solutions at pH 6.3 and 11.0 through the slow evaporation method at room temperature for about 1 week. The two histidine samples were designated as His6.3 and His11.0. These recrystallized histidine samples were then packed into 3.2 mm MAS rotors for NMR measurements. The rotor-synchronized spin-echo pulse sequences are shown in Fig. 1, where the ^{15}N magnetization is enhanced through cross polarization from protons with a contact time during which the spin-lock fields for ^{1}H and ^{15}N fulfill the Hartmann-Hahn matching condition. The 2D ^{15}N-^{15}N homonuclear *J*-resolved spectra are recorded using the standard spin-echo pulse sequence as shown in Fig. 1a, where $t_1/2$ is set to a multiple of spinning periods. Fig. 1b shows the rotor-synchronized DBSE sequence, where $t_1/4$ has to be set to a multiple of spinning periods. All magic-angle-spinning (MAS) NMR spectra were acquired on a Bruker Avance 600.1 MHz NMR spectrometer using an NHMFL 3.2 mm Low-E triple-resonance biosolids MAS probe [35,36]. The sample spinning rate was controlled within 15.0 kHz ± 3 Hz by a Bruker pneumatic MAS unit. During the 1 ms CP contact time, a ^{1}H spin-lock field of 50 kHz was used and the ^{15}N B_1 field was ramped from 38 to 56 kHz [37]. The ^{15}N 180° pulse lengths were experimentally calibrated to be 9.0 μs. A SPINAL64 decoupling sequence [38] with a ^{1}H B_1 field of 83.3 kHz was used for proton decoupling during the entire spin-echo periods and the data acquisition time. 256 scans were used to accumulate the ^{15}N signals with a recycle delay of 10 s. The ^{15}N chemical shifts were referenced to the ^{15}N amino resonance of glycine at 33.5 ppm.

All fittings were performed using the KaleidaGraph software.

3. Results and discussion

Fig. 2 shows the ^{15}N CPMAS spectra of the His6.3 and His11.0 samples. At pH 6.3, a total of six resonances were observed at 249.3, 189.9, 176.6, 171.1, 47.7, and 41.5 ppm. These ^{15}N resonances were unambiguously assigned through the ^{13}C-^{13}C and ^{15}N-^{13}C correlation spectra as shown in supplemental material (Fig. S1) and are labeled in the spectrum, representing two tautomeric states, i.e. the neutral τ and charged states that coexist at this pH [39], while the neutral π state is absent. On the other hand, for His11.0, a total of six resonances were also observed at 252.9, 249.4, 171.2, 167.5, 96.3, and 41.5 ppm. Three of those resonances are virtually the same as for the neutral τ state in the His6.3 sample and thus can be assigned to the neutral τ state at pH 11.0, while the other three resonances belong to the neutral π state. Therefore, the neutral τ and π states coexist with no charged state for the histidine at pH 11.0.

Fig. 3 shows the ^{15}N 2D *J*-resolved spectrum for the His6.3 sample. From the slices in the right panel, it is clear that the linewidth is ~7–10 Hz and no *J*-splitting is visible, as if no *J*-couplings occur among three nitrogen sites for both tautomeric states by using the standard rotor-synchronized spin-echo sequence. Similar results were observed for the His11.0 sample as shown in supplemental material, Fig. S2.

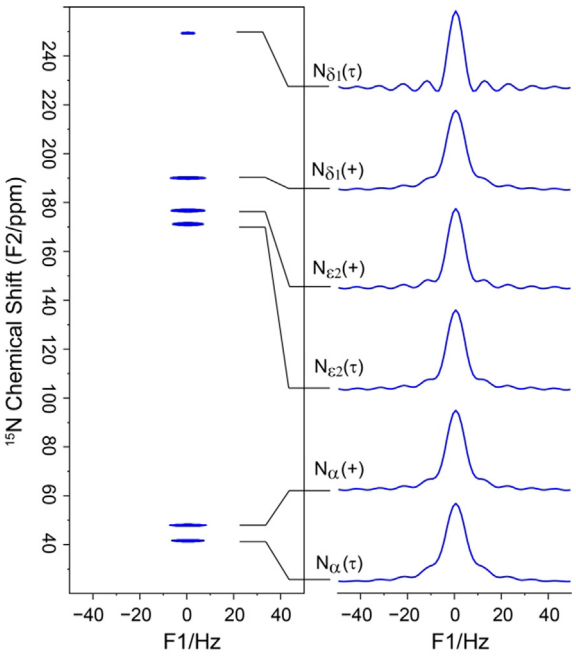

Fig. 3. ^{15}N 2D *J*-resolved spectrum (left) of His6.3 and their respective slices (right).

Considering how a dilute spin (e.g. ^{15}N) system with three homonuclear spins that are weakly coupled through *J*-couplings evolves during the DBSE sequence, the nuclear spin Hamiltonian in the usual rotating frame can be written as

$$H_Z = (\sum_{k=0}^{2} \Omega_k I_Z^k) + \sum_{i=0}^{1} \sum_{j=i+1}^{2} 2\pi J_{ij} I_Z^i I_Z^j \quad (1)$$

Here (I_X, I_Y, I_Z) are the spin operators, Ω_k represents the isotropic chemical shift for the k^{th} spin and the second term represents the *J*-couplings among these three spins. In this expression, the weak coupling limit has been applied [40], i.e. any *J*-coupling is much smaller than the chemical shift difference of the two spins involved, $|J_{ij}| \ll |\Omega_i - \Omega_j|$, and the dipolar interactions are completely suppressed by MAS as long as the MAS spinning rate does not fulfill the so-called rotational resonance condition [40], i.e. $\omega_r \neq |n(\Omega_k - \Omega_l)|, |n(\Omega_k - \Omega_m)|, |n(\Omega_m - \Omega_l)|$, where ω_r is the spinning speed and n is an integer number.

Under the DBSE sequences in Fig. 1b, the density matrix $\rho(t_1)$ is evolved from the initial density matrix $\rho(0)$ according to

$$\rho_{DBSE}(t_1)|_\phi = U_{DBSE}(\phi, t_1)\rho(0)U_{DBSE}^{+}(\phi, t_1) \quad (2)$$

Here, $U_{DBSE}(\phi, t_1) = e^{-iH_Z\frac{t_1}{4}}e^{-i\pi I_X}e^{-iH_Z\frac{t_1}{4}}e^{-i\phi I_X}e^{-iH_Z\frac{t_1}{4}}e^{-i\pi I_X}e^{-iH_Z\frac{t_1}{4}}$ is the unitary propagator. The time dependence of the signal for the k^{th} spin can thus be obtained by

$$S^k(t_1)|_\phi = trace\left(\left(I_X^k + iI_Y^k\right)\rho(t_1)|_\phi\right) \quad (3)$$

Here $\rho(0) = \sum_{k=0}^{2} I_X^k$, $I_X = \sum_{k=0}^{2} I_X^k$, and $I_Y = \sum_{k=0}^{2} I_Y^k$, while $\phi = 0$ or $\pi/2$ corresponding to without and with the red 90° pulse, respectively.

In the DBSE sequences of Fig. 1b, the chemical shift term is completely refocused in each spin echo period, thus only the *J*-coupling term is evolved during the spin echo periods. Thus the evolution of the *J*-modulated component at t_1 can be easily derived. The signal for the k^{th} spin evolved in Fig. 1b without the red 90° pulse is the same as in Fig. 1a:

$$S_{DBSE}^k(t_1)|_0 = trace\left(\left(I_X^k + iI_Y^k\right)\rho(t_1)|_0\right) = cos(\pi J_{kl}t_1)cos(\pi J_{km}t_1) \quad (4)$$

On the other hand, with the red 90° pulse in Fig. 1b the signal for the k^{th} spin becomes

$$\begin{aligned} S_{DBSE}^k(t_1)|_{\frac{\pi}{2}} &= trace\left(\left(I_X^k + iI_Y^k\right)\rho(t_1)|_{\frac{\pi}{2}}\right) \\ &= cos^2\left(\frac{\pi}{2}J_{kl}t_1\right)cos^2\left(\frac{\pi}{2}J_{km}t_1\right) \\ &\quad + sin^2\left(\frac{\pi}{2}J_{kl}t_1\right)cos\left(\frac{\pi}{2}J_{lm}t_1\right)cos\left(\frac{\pi}{2}J_{km}t_1\right) \\ &\quad + sin^2\left(\frac{\pi}{2}J_{km}t_1\right)cos\left(\frac{\pi}{2}J_{kl}t_1\right)cos\left(\frac{\pi}{2}J_{lm}t_1\right) \end{aligned} \quad (5)$$

Here, $l = \mathrm{mod}(k+1,3)$ and $m = \mathrm{mod}(k+2,3)$ representing the other two spins that are *J*-coupled with the k^{th} spin.

For each tautomeric state in histidine (Scheme 1), there are three nitrogen sites (N_α, $N_{\delta1}$, and $N_{\varepsilon2}$), where $N_{\delta1}$ and $N_{\varepsilon2}$ are separated by two covalent bonds, and N_α and $N_{\delta1}$ are not bonded directly, but may be connected through a hydrogen bond, while N_α and $N_{\varepsilon2}$ are far away. For such a three-spin system, we use Scheme 2 to depict the possible coupling network in histidine, where $^2J_{N\delta1N\varepsilon2}$ represents the two-bond *J*-coupling between $N_{\delta1}$ and $N_{\varepsilon2}$ and $^{2h}J_{N\delta1N\alpha}$ stands for the potential intramolecular hydrogen-bond mediated *J*-coupling, while no *J*-coupling is expected between N_α and $N_{\varepsilon2}$. There is no intermolecular $^{2h}J_{N\delta1N\alpha}$ since the N_α-$N_{\delta1}$ distance from two closest molecules was more than 5 Å according to the crystal structure [41]. When k = 0, 1, and 2 in Eq. (5) refers to N_α, $N_{\delta1}$, and $N_{\varepsilon2}$ respectively, we have $J_{01}=^{2h}J_{N\delta1N\alpha}$, $J_{02} = J_{N\alpha N\varepsilon2} = 0$, and $J_{12}=^2J_{N\delta1N\varepsilon2}$ based on Scheme 2. Therefore, the obtained signals $S_{DBSE}^k(t_1)|_0$ and $S_{DBSE}^k(t_1)|_{\frac{\pi}{2}}$ under the DBSE sequence without and with the red 90° pulse can be simplified from Eqs. (4) and (5) and listed in Table 1.

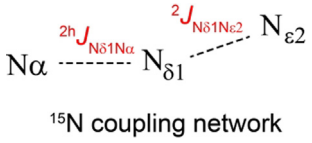

Scheme 2.

It is clear from Table 1 that $S_{DBSE}^k(t_1)|_0 = S_{DBSE}^k(t_1)|_{\frac{\pi}{2}} = 1$ when there are no *J*-couplings between the different nitrogen sites. In other words, the observed signals with and without the 90° pulse should be the same when $^{2h}J_{N_{\delta1}N_\alpha} = {}^2J_{N_{\delta1}N_{\varepsilon2}} = 0$. If there exists any *J*-coupling, the observed signals with and without the 90° pulse should have a different functional relationship with $^{2h}J_{N_{\delta1}N_\alpha}$ and $^2J_{N_{\delta1}N_{\varepsilon2}}$. It is worth noting that, for N_α and $N_{\varepsilon2}$, $S_{DBSE}^{N_\alpha/N_{\varepsilon2}}(t_1)|_0$ depends solely on their *J*-coupling with the nearby nitrogen $N_{\delta1}$, while $S_{DBSE}^{N_\alpha/N_{\varepsilon2}}(t_1)|_{\frac{\pi}{2}}$ depends not only on the *J*-coupling with its nearby nitrogen $N_{\delta1}$, but also on the *J*-coupling between the nitrogen $N_{\delta1}$ and the other nitrogen, although this contribution is as if it was one-half of their *J*-coupling.

Fig. 4 shows the ^{15}N DBSE spectra of the His6.3 sample at t_1 = 80 ms without and with the red 90° pulse. It is apparent from this figure that, for the charged state, the N_α(+) signal intensity remains unchanged without and with the red 90° pulse, while the signal intensities for $N_{\delta1}$(+) and $N_{\varepsilon2}$(+) are slightly increased when the red 90° pulse is applied. On the other hand, the nitrogen signals for the neutral τ state gain intensity when the 90° pulse is applied, especially for $N_{\delta1}$(τ) and N_α(τ). This observation implies that there may be a weak two-bond $^2J_{N\delta1(+)N\varepsilon2(+)}$ in the charged state, while there exist relatively strong *J*-couplings between three nitrogen sites in the neutral τ state.

Since both $S_{DBSE}^k(t_1)|_0$ and $S_{DBSE}^k(t_1)|_{\frac{\pi}{2}}$ are evolved over the same t_1 period, their ratio $R_{DBSE}^k(t_1) = S_{DBSE}^k(t_1)|_0 / S_{DBSE}^k(t_1)|_{\frac{\pi}{2}}$ eliminates the transverse dephasing effects and depends solely on the *J*-couplings. Fig. 5 shows the plots of $R_{DBSE}^k(t_1)$ as a function of t_1 for all six ^{15}N resonances from the His6.3 sample. Clearly, $R_{DBSE}^{N_\alpha(+)}(t_1)$ for N_α(+) remains one over the entire echo time t_1, i.e. $^{2h}J_{N_{\delta1}(+)N_\alpha(+)} = 0$, confirming that the N_α(+) in the charged state does not exhibit the hydrogen-bond mediated *J*-coupling with $N_{\delta1}$(+). However, the ratios for $N_{\delta1}$(+) and $N_{\varepsilon2}$(+) show a slight decrease with increasing t_1. Using $^{2h}J_{N_{\delta1}(+)N_\alpha(+)} = 0$ as a constant, we fitted these $R_{DBSE}^{N_{\varepsilon2}(+)/N_{\delta1}(+)}(t_1)$ for $N_{\varepsilon2}$(+) and $N_{\delta1}$(+) as a function of t_1 based on the formula in Table 1, yielding a two-bonded $^2J_{N_{\delta1}(+)N_{\varepsilon2}(+)}$ of 0.89 ± 0.09 Hz and 1.10 ± 0.11 Hz, respectively. Thus, the mean of these two values becomes $^2J_{N_{\delta1}(+)N_{\varepsilon2}(+)}$ = 1.0 ± 0.2 Hz, consistent with the two-bonded *J*-coupling constant obtained from the selective measurements [28].

On the other hand, the ratios for all three nitrogen sites in the neutral τ state decrease dramatically as a function of t_1 as compared to that in the charged state, indicating that there exist *J*-couplings in the ^{15}N coupling network of the neutral τ state of histidine. In particular, $R_{DBSE}^{N_\alpha(\tau)}(t_1)$ depends more dramatically on the echo time t_1 than $R_{DBSE}^{N_{\varepsilon2}(\tau)}(t_1)$. It is thus expected that $^{2h}J_{N_{\delta1}(\tau)N_\alpha(\tau)}$ should be larger than $^2J_{N_{\delta1}(\tau)N_{\varepsilon2}(\tau)}$. As discussed in Table 1, the effect of $^2J_{N_{\delta1}(\tau)N_{\varepsilon2}(\tau)}$ on $S_{DBSE}^{N_\alpha(\tau)}(t_1)|_{90^\circ}$ is far less than that of $^{2h}J_{N_{\delta1}(\tau)N_\alpha(\tau)}$ on $S_{DBSE}^{N_{\varepsilon2}(\tau)}(t_1)|_{90^\circ}$. Therefore, we first

Table 1
Each ^{15}N signal at the end of the DBSE period without and with the 90° pulse.

Spin k	$S^k_{DBSE}(t_1)\|_0$	$S^k_{DBSE}(t_1)\|_{\frac{\pi}{2}}$
0 or N_α	$cos(\pi\ {}^{2h}J_{N_{\delta1}N_\alpha}t_1)$	$1-2sin^2(\frac{\pi}{2}\ {}^{2h}J_{N_{\delta1}N_\alpha}t_1)sin^2(\frac{\pi}{4}\ {}^{2}J_{N_{\delta1}N_{\varepsilon2}}t_1)$
1 or $N_{\delta1}$	$cos(\pi\ {}^{2h}J_{N_{\delta1}N_\alpha}t_1)cos(\pi\ {}^{2}J_{N_{\delta1}N_{\varepsilon2}}t_1)$	$cos^2(\frac{\pi}{2}\ {}^{2h}J_{N_{\delta1}N_\alpha}t_1)cos^2(\frac{\pi}{2}\ {}^{2}J_{N_{\delta1}N_{\varepsilon2}}t_1)+sin^2(\frac{\pi}{2}\ {}^{2h}J_{N_{\delta1}N_\alpha}t_1)cos(\frac{\pi}{2}\ {}^{2}J_{N_{\delta1}N_{\varepsilon2}}t_1)+sin^2(\frac{\pi}{2}\ {}^{2}J_{N_{\delta1}N_{\varepsilon2}}t_1)cos(\frac{\pi}{2}\ {}^{2h}J_{N_{\delta1}N_{\varepsilon2}}t_1)$
2 or $N_{\varepsilon2}$	$cos(\pi\ {}^{2}J_{N_{\delta1}N_{\varepsilon2}}t_1)$	$1-2sin^2(\frac{\pi}{2}\ {}^{2}J_{N_{\delta1}N_{\varepsilon2}}t_1)sin^2(\frac{\pi}{4}\ {}^{2h}J_{N_{\delta1}N_\alpha}t_1)$

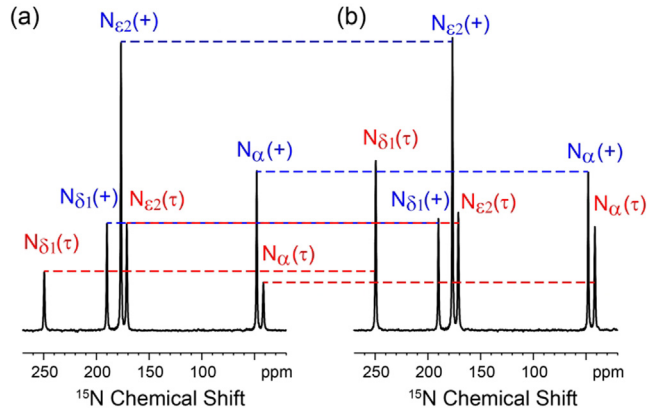

Fig. 4. ^{15}N DBSE spectra of the histidine powder (at pH 6.3) at t_1 = 80 ms without (a) and with (b) the red 90° pulse. The resonances for the neutral τ and charged states are differentiated by τ and +.

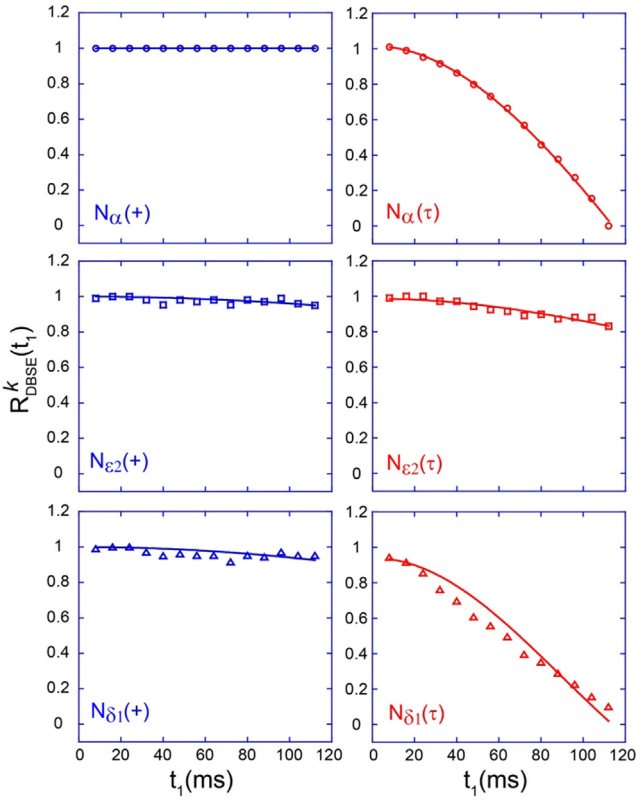

Fig. 5. Plots of R^k_{DBSE} (t_1) as a function of the echo time t_1 for all six nitrogen resonances from the His6.3 sample, where k refers to N_α, $N_{\varepsilon2}$, and $N_{\delta1}$.

set ${}^{2}J_{N_{\delta1}(\tau)N_{\varepsilon2}(\tau)}$ = 1.1 Hz (i.e. taking the J-coupling value from the charged state) and used ${}^{2h}J_{N_{\delta1}(\tau)N_\alpha(\tau)}$ as a variable to fit the time dependence of $R^{N_\alpha(\tau)}_{DBSE}$ (t_1). We then used the obtained ${}^{2h}J_{N_{\delta1}(\tau)N_\alpha(\tau)}$ value as a constant and ${}^{2}J_{N_{\delta1}(\tau)N_{\varepsilon2}(\tau)}$ as a variable to fit $R^{N_{\varepsilon2}(\tau)}_{DBSE}$ (t_1). By reiterating this procedure several times, we could get the variables ${}^{2h}J_{N_{\delta1}(\tau)N_\alpha(\tau)}$ and ${}^{2}J_{N_{\delta1}(\tau)N_{\varepsilon2}(\tau)}$ converged to ${}^{2h}J_{N_{\delta1}(\tau)N_\alpha(\tau)}$ = 4.38 ± 0.02 Hz and ${}^{2}J_{N_{\delta1}(\tau)N_{\varepsilon2}(\tau)}$ = 1.82 ± 0.05 Hz. As shown in Fig. 5, the solid lines fit the experimental data quite well. Using these values as constants, we can obtain the echo-time dependence of $R^{N_{\delta1}(\tau)}_{DBSE}$($t_1$) based on the formula in Table 1 and the theoretical curve agrees with the experimental data reasonably well, as illustrated in Fig. 5. Note that with this procedure there was only a single variable in each fitting and the error bars were directly obtained from the fittings.

Fig. 6 shows the plots of the time dependence R^k_{DBSE} (t_1) for all six ^{15}N resonances from the His11.0 sample. Clearly, the ratios for $N_\alpha(\tau)$ and $N_{\delta1}(\tau)$ in the neutral τ state decrease dramatically as a function of t_1, as compared to that for $N_{\varepsilon2}(\tau)$. By using the same procedure as in Fig. 5 to fit the $N_\alpha(\tau)$ and $N_{\varepsilon2}(\tau)$ data, we obtained ${}^{2h}J_{N_{\delta1}(\tau)N_\alpha(\tau)}$ = 4.53 ± 0.03 Hz and ${}^{2}J_{N_{\delta1}(\tau)N_{\varepsilon2}(\tau)}$ = 1.75 ± 0.05 Hz. Again, with these values as constants, as illustrated in Fig. 6, the theoretically obtained echo-time dependence $R^{N_{\delta1}(\tau)}_{DBSE}$($t_1$) agrees well with the experimental data. Interestingly, the neutral τ state for histidine at different pHs (pH 6.3 and 11.0) exhibits virtually the same ${}^{2h}J_{N_{\delta1}(\tau)N_\alpha(\tau)}$, ${}^{2}J_{N_{\delta1}(\tau)N_{\varepsilon2}(\tau)}$, and chemical shifts for $N_\alpha(\tau)$

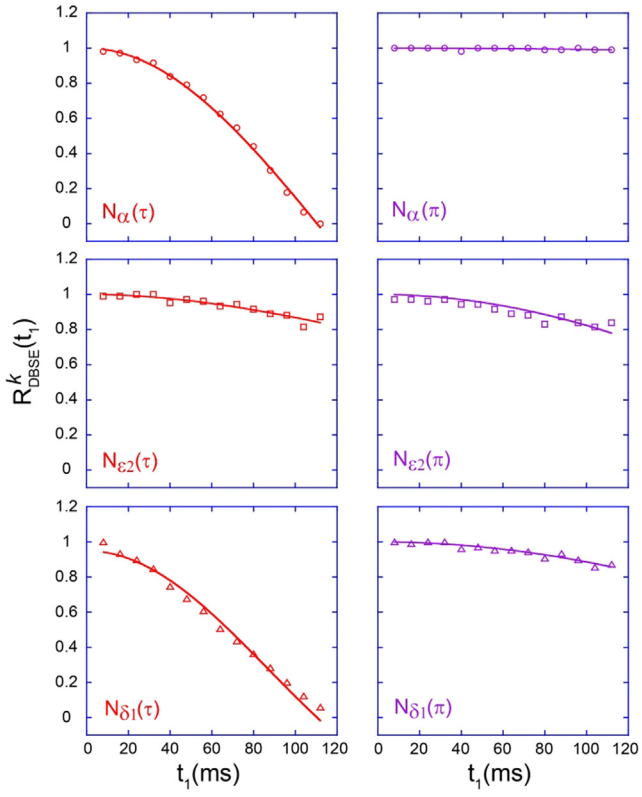

Fig. 6. Plots of R^k_{DBSE} (t_1) as a function of the echo time t_1 for all six nitrogen resonances from the His11.0 sample, where k refers to N_α, $N_{\varepsilon2}$, and $N_{\delta1}$.

Table 2
The measured *J*-coupling constants for the His6.3 and His11.0 samples.

	His6.3		His11.0	
	Charged state	Neutral τ state	Neutral τ state	Neutral π state
$^{2h}J_{N_\alpha N_{\delta1}}$(Hz)	0	4.38 ± 0.02	4.53 ± 0.03	0.39 ± 0.07
$^{2}J_{N_{\delta1}N_{\varepsilon2}}$(Hz)	1.0 ± 0.2	1.82 ± 0.05	1.75 ± 0.05	1.92 ± 0.08

and $N_{\delta1}(\tau)$ nitrogen sites, although there exists a small chemical shift difference for the $N_{\varepsilon2}(\tau)$ site, suggesting that the structure for the neutral τ state is not sensitive to the preparation condition at different pHs.

By comparison, the time-dependences of R^{k}_{DBSE} (t_1) for the neutral π state in the His11.0 sample are rather moderate. Interestingly, $R^{N_\alpha(\pi)}_{DBSE}$ (t_1) does decrease slightly over the echo time, indicating that there may exist an extremely weak hydrogen-bond mediated *J*-coupling, if any, between $N_\alpha(\pi)$ and $N_{\delta1}(\pi)$. By using the similar procedure to fit the $N_\alpha(\pi)$ and $N_{\varepsilon2}(\pi)$ data, we could obtain $^{2h}J_{N_{\delta1}(\pi)N_\alpha(\pi)} = 0.39 \pm 0.07$ Hz and $^{2}J_{N_{\delta1}(\pi)N_{\varepsilon2}(\pi)} = 1.92 \pm 0.08$ Hz. With these two values as constants, the time dependent $R^{N_{\delta1}(\pi)}_{DBSE}$ (t_1) is highly consistent with the experimental data, as illustrated in Fig. 6. Table 2 summarizes the *J*-coupling constants for the His6.3 and His11.0 samples measured with our DBSE sequence.

It is important to note that, with the DBSE sequence, very weak *J*-couplings (<1 Hz) could still be obtained even if the observed linewidths in the *J*-resolved spectrum in Fig. 2 are as large as 10 Hz. This is because the transverse dephasing effects during the *J*-evolution in the spin-echo periods have been eliminated in the ratio of the DBSE signals with and without the 90° pulse, as compared to the standard *J*-resolved spin-echo experiments where the *J*-evolution and spin-spin relaxation are mixed together such that *J*-splittings become invisible in the *J*-resolved spectra when the *J*-coupling value is much less than the observed linewidth. This is indicated in the time domain data for the 2D *J*-resolved spectra shown in Fig. S5 where the transverse dephasings are dominated, such that the *J*-coupling induced decay can hardly be observed.

4. Conclusion

In summary, we have used the double spin-echo pulse sequence with and without the 90° pulse in between the two spin-echo periods to measure weak ^{15}N-^{15}N homonuclear scalar couplings in the ^{13}C,^{15}N labeled histidine samples at pH 6.3 and 11.0, having a mixture of different tautomeric states. For the charged state, the measured two-bond $^{2}J_{N\delta1(+)N\varepsilon2(+)}$ value in the imidazole ring was ~1.0 Hz, while for both neutral τ and π states, the obtained two-bond $^{2}J_{N\delta1N\varepsilon2}$ value in the imidazole ring was ~1.90 Hz, almost twice that of the charged state. This suggests that the bond angle $\angle N_{\delta1}C_{\varepsilon1}N_{\varepsilon2}$ in the imidazole ring may be different between the neutral and charge states. Since the *J*-couplings are highly correlated with redistributions of electron densities through bonds, this difference in this two-bond *J*-coupling could be used to refine detailed local structural models through theoretical calculations [18,42]. For the charged state, there is no hydrogen-bond mediated *J*-coupling between $N_\alpha(+)$ and $N_{\delta1}(+)$ sites. However, there exists the hydrogen-bond mediated *J*-coupling between N_α and $N_{\delta1}$ sites for both neutral states. For the neutral τ state, the hydrogen-bond mediated $^{2h}J_{N\delta1(\tau)N\alpha(\tau)}$ value of 4.38 ± 0.02 Hz between the $N_{\delta1}(\tau)$ site in the imidazole ring and the backbone $N_\alpha(\tau)$ site in the neutral τ state was obtained, directly confirming the presence of the $N_\alpha(\tau)\cdots H\cdots N_{\delta1}(\tau)$ hydrogen bond. Such a hydrogen-bond formation was suggested through the ^{1}H-^{15}N correlation spectrum and the ^{15}N-^{1}H distance measurement [11]. However, this obtained $^{2h}J_{N\delta1(\tau)N\alpha(\tau)}$ value of 4.38 ± 0.02 Hz is about half of the values observed in other compounds [23–25], implying that this $N_\alpha(\tau)\cdots H\cdots N_{\delta1}(\tau)$ hydrogen bond in histidine is relatively weak, partly due to the fast rotation of the charged amine group. While the hydrogen-bond mediated $^{2h}J_{N\delta1(\pi)N\alpha(\pi)}$ between the $N_{\delta1}$ site in the imidazole ring and the backbone N_α site in the neutral π state was just 0.39 ± 0.07 Hz, indicating the presence of a very weak $N_\alpha(\pi)\cdots H\cdots N_{\delta1}(\pi)$ hydrogen bond in the neutral π state. More importantly, this newly proposed double spin-echo pulse sequence is capable of measuring weak *J*-couplings, even if whose values are much smaller than the observed linewidths, owing to the fact that the transverse dephasing effects are completely eliminated during the period of *J*-evolution. This is particularly useful and is applicable in highly heterogeneous systems such as disorder solids [43,44]. Therefore, it is anticipated that this proposed methodology would open up a new way of investigating homonuclear *J*-coupling networks in disorder solids and highly heterogeneous biological systems [45–49].

Declaration of Competing Interest

The authors declare that they have no known competing financial interests or personal relationships that could have appeared to influence the work reported in this paper.

Acknowledgement

This work was supported in part by NIH grant AI023007. We thank Dr. Yimin Miao at Florida State University for preparing the histidine samples. All NMR experiments were carried out at the National High Magnetic Field Lab (NHMFL) supported by the NSF Cooperative Agreement DMR-1644779 and the State of Florida. X.P. acknowledges the financial support from the National Natural Science Foundation of China (No. 11927811). C.H.T. thanks to the financial support from the China Scholarship Council for visiting the NHMFL. C.Z. acknowledges the National Natural Science Foundation of China (No. 11761141010).

Appendix A. Supplementary material

2D ^{15}N-^{13}C and ^{13}C-^{13}C correlation spectra of the histidine at pH6.3 for resonance assignments; ^{15}N 2D *J*-resolved spectrum of the histidine at pH 11.0 and their respective slices; representatives of intra- and inter-molecular N_α-$N_{\delta1}$ distances; ^{15}N DBSE spectra of His11.0 at t_1 = 112 ms; the time-domain data of the 2D *J*-resolved spectra. Supplementary data to this article can be found online at https://doi.org/10.1016/j.jmr.2020.106757.

References

[1] M. Hennig, B.H. Geierstranger, Direct detection of a histidine-histidine side chain hydrogen bond important for folding of apomyoglobin, J. Am. Chem. Soc. 121 (1999) 5123–5126.
[2] J.L. Markley, Observation of histidine residues in proteins by means of nuclear magnetic-resonance spectroscopy, Acc. Chem. Res. 8 (1975) 70–80.
[3] B.S. Perrin Jr., Y. Tian, R. Fu, C.V. Grant, E.Y. Chekmenev, W.E. Wieczorek, A.E. Dao, R.M. Hayden, C.M. Burzynski, R.M. Venable, M. Sharma, S.J. Opella, R.W. Pastor, M.L. Cotten, High-resolution structures and orientations of antimicrobial peptides piscidin 1 and piscidin 3 in fluid bilayers reveal

tilting, kinking, and bilayer immersion, J. Am. Chem. Soc. 136 (2014) 3491–3504.
[4] J. Hu, R. Fu, K. Nishimura, L. Zhang, H.X. Zhou, D.D. Busath, V. Vijayvergiya, T.A. Cross, Histidines, heart of the hydrogen ion channel from influenza A virus: Toward an understanding of conductance and proton selectivity, Proc. Natl. Acad. Sci. USA 103 (2006) 6865–6870.
[5] M. Sharma, M. Yi, H. Dong, H. Qin, E. Peterson, D.D. Busath, H.X. Zhou, T.A. Cross, Insight into the mechanism of the influenza A proton channel from a structure in a lipid bilayer, Science 330 (2010) 509–512.
[6] H. Eckert, J.P. Yesinowski, L.A. Silver, E.M. Stolper, Water in silicate glasses: Quantitation and structural stidies by proton solid echo and magic angle spinning NMR methods, J. Phys. Chem. 92 (1988) 2055–2064.
[7] G.S. Harbison, J. Herzfeld, R.G. Griffin, J. Am. Chem. Soc. 103 (1981) 4752–4754.
[8] M. Munowitz, W.W. Bachovchin, J. Herzfeld, C.M. Dobson, R.G. Griffin, Acid-base and tautomeric equilibria in the solid-state - N-15 NMR-spectroscopy of histidine and imidazole, J. Am. Chem. Soc. 104 (1982) 1192–1196.
[9] Y.F. Wei, A.C. de Dios, A.E. McDermott, J. Am. Chem. Soc. 121 (1999) 10389–10394.
[10] X.J. Song, A.E. McDermott, Proton transfer dynamics and N—H bond lengtheningin N—H···N model systems: a solid-state NMR study, Magn. Reson. Chem. 39 (2001) S37–43.
[11] S.H. Li, M. Hong, Protonation, tautomerization, and rotameric structure of histidine: a comprehensive study by magic-angle-spinning solid-state NMR, J. Am. Chem. Soc. 133 (2011) 1534–1544.
[12] B. Henry, P. Tekely, J.J. Delpuech, pH and pK determinations by high-resolution solid-state C-13 NMR: acid-base and tautomeric equilibria of lyophilized L-histidine, J. Am. Chem. Soc. 124 (2002) 2025–2034.
[13] G.A. Morris, R. Freeman, Enhancement of nuclear magnetic resonance signals by polarization transfer, J. Am. Chem. Soc. 101 (1979) 760–762.
[14] A. Bax, R. Freeman, S.P. Kempsel, Natural abundance carbon-13-carbon-13 coupling observed via double-quantum coherence, J. Am. Chem. Soc. 102 (1980) 4849–4851.
[15] F. Fayon, D. Massiot, M.H. Levitt, J.J. Titman, D.H. Gregory, L. Duma, L. Emsley, S.P. Brown, Through-space contributions to two-dimensional double-quantum J correlation NMR spectra of magic-angle-spinning solids, J. Chem. Phys. 122 (2005) 194313.
[16] S.J. Grabowski, What is the covalency of hydrogen bonding?, Chem Rev. 111 (2011) 2597–2625.
[17] A.J. Dingley, F. Cordier, S. Grzesiek, An introduction to hydrogen bond scalar couplings, Concepts Magnetic Resonance 13 (2001) 103–127.
[18] S.A. Joyce, J.R. Yates, C.J. Pickard, S.P. Brown, Density functional theory calculations of hydrogen-bond-mediated NMR J coupling in the solid state, J. Am. Chem. Soc. 130 (2008) 12663–12670.
[19] J.B. Blake, M.W.W. Adam, M.F. Summers, Novel observation of NH-S(Cys) hydrogen-bond-mediated scalar coupling in ^{113}Cd-substituted rubredoxin from pyrococcus furiosus, J. Am. Chem. Soc. 114 (1992) 4931–4933.
[20] A.J. Dingley, S. Grzesiek, Direct observation of hydrogen bonds in nucleic acid base pairs by internucleotide $^{2}J_{NN}$ couplings, J. Am. Chem. Soc. 120 (1998) 8293–8297.
[21] K. Pervushin, A. Ono, C. Fernandez, T. Szyperski, M. Kainosho, K. Wuthrich, NMR scalar couplings across Watson!Crick base pair hydrogen bonds in DNA observed by transverse relaxation-optimized spectroscopy, Proc. Natl. Acad. Sci. USA 95 (1998) 14147–14151.
[22] G. Cornilescu, J.S. Hu, A. Bax, Identification of the hydrogen bonding network in a protein by scalar couplings, J. Am. Chem. Soc. 121 (1999) 2949–2950.
[23] S.P. Brown, M. Perez-Torralba, D. Sanz, R.M. Claramunt, L. Emsley, Determining hydrogen-bond strengths in the solid state by NMR: the quantitative measurement of homonuclear *J* couplings, Chem. Commun. (2002) 1852–1853.
[24] S.P. Brown, M. Perez-Torralba, D. Sanz, R.M. Claramunt, L. Emsley, The direct detection of a hydrogen bond in the solid state by NMR through the observation of a hydrogen-bond mediated 15N–15N J coupling, J. Am. Chem. Soc. 124 (2002) 1152–1153.
[25] T.N. Pham, J.M. Griffin, S. Masiero, S. Lena, G. Gottarelli, P. Hodgkinson, C. Filip, S.P. Brown, Quantifying hydrogen-bonding strength: the measurement of $^{2h}J_{NN}$ couplings in self-assembled guanosines by solid-state ^{15}N spin-echo MAS NMR, Phys. Chem. Chem. Phys. 9 (2007) 3416–3423.
[26] S. Glanzer, K. Zangger, Visualizing unresolved scalar couplings by real-time J-upscaled NMR, J. Am. Chem. Soc. 137 (2015) 5163–5169.
[27] W.P. Aue, J. Karhan, R.R. Ernst, Homonuclear broad band decoupling and two-dimensional J-resolved NMR spectroscopy, J. Chem. Phys. 64 (1976) 4226–4227.
[28] P. Thureau, G. Mollica, F. Ziarelli, S. Viel, Selective measurements of long-range homonuclear J-couplings in solid-state NMR, J. Magn. Reson. 231 (2013) 90–94.
[29] K. Takegoshi, K. Ogura, K. Hikichi, A perfect spin echo in a weakly homonuclear *J*-coupled two spin-1/2 system, J. Magn. Reson. 84 (1989) 611–615.
[30] P.C.M. van Zijl, C.T.W. Moonen, M. von Kienlin, Homonuclear *J* refocusing in Echo Spectroscopy, J. Magn. Reson. 89 (1990) 28–40.
[31] T. Gullion, J. Schaefer, Rotational-echo double-resonance NMR, J. Magn. Reson. 81 (1989) 196.
[32] J. Trebosc, J.P. Amoureux, L. Delevoye, J.W. Wiench, M. Pruski, Frequency-selective measurement of heteronuclear scalar couplings in solid-state NMR, Solid State Sci. 6 (2004) 1089–1095.
[33] I. Hung, A.C. Uldry, J. Becker-Baldus, A.L. Webber, A. Wong, M.E. Smith, S.A. Joyce, J.R. Yates, C.J. Pickard, R. Dupree, S.P. Brown, Probing heteronuclear ^{15}N–^{17}O and ^{13}C–^{17}O connectivities and proximities by solid-state NMR spectroscopy, J. Am. Chem. Soc. 131 (2009) 1820–1834.
[34] A.L. Webber, J.R. Yates, M. Zilka, S. Sturniolo, A.C. Uldry, A.K. Corlett, C.J. Pickard, M. Perez-Torralba, M.A. Garcia, D.S. Maria, R.M. Claramunt, S.P. Brown, Weak intermolecular CH···N hydrogen bonding: determination of ^{13}CH–^{15}N hydrogen-bond mediated J couplings by solid-state NMR spectroscopy and first-principles calculations, J. Phys. Chem. A 124 (2020) 560–572.
[35] P.L. Gor'kov, E.Y. Chekmenev, M. Cotten, J.J. Buffy, N.J. Traaseth, G. Veglia, W.W. Brey, Using low-E resonators to reduce RF heating in biological samples for static solid-state NMR up to 900 MHz, J. Magn. Reson. 185 (2007) 77–93.
[36] S.A. McNeill, P.L. Gor'kov, K. Shetty, W.W. Brey, J.R. Long, A low-E magic angle spinning probe for biological solid state NMR at 750 MHz, J. Magn. Reson. 197 (2009) 135–144.
[37] O.B. Peersen, X.L. Wu, S.O. Smith, Enhancement of CP-MAS signals by variable-amplitude cross-polarization - compensation for inhomogeneous B-1 fields, J. Magn. Reson. A 106 (1994) 127–131.
[38] B.M. Fung, A.K. Khitrin, K. Ermolaev, An improved broadband decoupling sequence for liquid crystals and solids, J. Magn. Reson. 142 (2000) 97–101.
[39] Y. Miao, T.A. Cross, R. Fu, Differentiation of histidine tautomeric states using ^{15}N selectively filtered ^{13}C solid-state NMR spectroscopy, J. Magn. Reson. 245 (2014) 105–109.
[40] L. Duma, W.C. Lai, M. Carravetta, L. Emsley, S.P. Brown, M.H. Levitt, Principles of spin-echo modulation by *J*-couplings in magic-angle-spinning solid-state NMR, ChemPhysChem 5 (2004) 815–833.
[41] J.J. Madden, E.L. McGandy, N.C. Seeman, The crystal structure of the monodinie form of L-histidine, Acta Cryst. B 28 (1972) 2382–2389.
[42] C.E. Hughes, G.N.M. Reddy, S. Masiero, S.P. Brown, P.A. Williams, K.D.M. Harris, Determination of a complex crystal structure in the absence of single crystals: analysis of powder X-ray diffraction data, guided by solid-state NMR and periodic DFT calculations, reveals a new 2'-deoxyguanosine structural motif, Chem. Sci. 8 (2017) 3971–3979.
[43] S. Cadars, A. Lesage, M. Trierweiler, L. Heux, L. Emsley, NMR measurements of scalar-coupling distributions in disordered solids, Phys. Chem. Chem. Phys. 9 (2007) 92–103.
[44] P. Guerry, M.E. Smith, S.P. Brown, ^{31}P MAS refocused INADEQUATE Spin-Echo (REINE) NMR spectroscopy: revealing J coupling and chemical shift two-dimensional correlations in disordered solids, J. Am. Chem. Soc. 131 (2009) 11861–11874.
[45] Y. Miao, R. Fu, H.X. Zhou, T.A. Cross, Dynamic short hydrogen bonds in histidine tetrad of full length M2 proton channel reveal tetrameric structural heterogeneity and functional mechanism, Structure 23 (2015) 2300–2308.
[46] R. Fu, Y. Miao, H. Qin, T.A. Cross, Observation of the imidazole-imidazolium hydrogen bonds responsible for selective proton conductance in the influenza A M2 channel, J. Am. Chem. Soc. 142 (2020) 2115–2119.
[47] K.T. Movellan, M. Wegstroth, K. Overkamp, A. Leonov, S. Becker, L.B. Andreas, Imidazole-imidazole hydrogen bonding in the pH-sensing histidine side chains of influenza A M2, J. Am. Chem. Soc. 142 (2020) 2704–2708.
[48] F. Hu, W.B. Luo, M. Hong, Mechanisms of proton conduction and gating in influenza M2 proton channels from solid-state NMR, Science 330 (2010) 505–508.
[49] M. Hong, K.J. Fritzsching, J.K. William, Hydrogen-bonding partner of the proton-conducting histidine in the influenza M2 proton channel revealed from ^{1}H chemical shifts, J. Am. Chem. Soc. 134 (2012) 14753–14755.